On the importance of wall transpiration in wall-modeled LES of nonequilibrium flows

By T. Salomone, M. P. Whitmore AND S. T. Bose

Abstract

Numerical simulations of high-Reynolds-number flows present significant challenges, particularly in predicting separated flows induced by mild adverse pressure gradients. Both equilibrium and nonequilibrium wall models can accurately predict small separation bubbles, but they have required resolving (or nearly resolving) a viscous sublayer induced by the finite pressure gradient near the separation point. Generally, both equilibrium and nonequilibrium wall models impose no-penetration conditions. Lighthill (1958) demonstrated that a wall-normal transpiration velocity naturally arises when matching the viscous boundary layer with the inviscid outer flow at high Reynolds numbers. Building on this result, we present an alternative derivation of the large-eddy simulation wall boundary condition that shows the necessity of wall transpiration in the limit of coarse resolution. Specifically, we show that this formulation satisfies the no-slip limit ($\Delta^+ \ll 1$) and recover Lighthill's viscous correction to the inviscid equations when $\Delta \gg \delta$. Under certain assumptions, it is then possible to show that this boundary condition is equivalent to a slip wall model formulation, first introduced by Bose & Moin (2014). Preliminary simulations of the NASA/Boeing Gaussian bump show favorable comparisons of the surface pressure and skin friction with available direct numerical simulations and experimental measurements.

1. Introduction

Turbulent flows subjected to pressure gradients are common in many engineering applications, such as the flow over an airplane wing, the design of turbomachinery, and the performance of diffusers and nozzles. These flows are of particular interest because of the presence of acceleration regions (associated with peak pressure coefficients) and flow separation, both of which must be accurately captured. Predicting high-Reynolds-number flows under the influence of pressure gradients remains a major challenge for current numerical methods, largely because of the high computational cost involved. Most of this cost is associated with resolving the inner portion of the boundary layer, whose resolution requirements grow rapidly with Reynolds number (Choi & Moin 2012; Yang & Griffin 2021). Recent studies have demonstrated that, in flows with separation or curvature, the grid density required to recover the correct pressure scaling increases locally as $Re^{4/3}$ (Agrawal *et al.* 2024a). As a result, direct numerical simulation (DNS) and wall-resolved large-eddy simulation (WRLES) are feasible only at low to moderate Reynolds numbers. Wall-modeled large-eddy simulation (WMLES), by contrast, circumvents this limitation by modeling the near-wall region, making simulations at high Reynolds numbers more tractable.

In most WMLES, the wall is treated with a no-penetration condition ($v = 0$), and

the viscous wall shear stress (τ_w) is specified. This stress is typically computed from the resolved outer-layer flow quantities, allowing the coarse LES grid to represent the correct momentum exchange at the wall without resolving the viscous sublayer. The most widely used wall models, such as the equilibrium wall-stress model (EQWM), assume a steady, attached boundary layer in a local equilibrium state either through the assumption of a reduced stress balance equation or directly through a velocity distribution (Cabot & Moin 1999). These EQWMs perform well in zero-pressure-gradient boundary layers, but they lose accuracy in nonequilibrium conditions, where curvature or pressure gradients strongly affect the near-wall dynamics (Whitmore *et al.* 2021, 2022; Agrawal *et al.* 2024a).

Nonequilibrium wall models have also been developed to improve the prediction of wall stress under strong pressure gradients (Balaras *et al.* 1996; Park & Moin 2014; Fowler *et al.* 2022, 2023; Agrawal *et al.* 2024b). However, these approaches often increase methodological complexity—for example, by requiring separate treatments for the wall and outer regions (Balaras *et al.* 1996), by solving additional evolution equations for the wall stress (Fowler *et al.* 2022, 2023), or by introducing special treatments for the eddy viscosity (Park & Moin 2014; Agrawal *et al.* 2024b). Moreover, their performance at high Reynolds numbers has not yet been shown to scale favorably.

An alternative approach is provided by the slip wall model, which derives a wall boundary condition directly from the Navier–Stokes equations under the assumption of a differential filter (Bose & Moin 2014; Bae *et al.* 2019). This boundary condition admits a finite Reynolds shear stress at the wall due to the presence of instantaneous wall transpiration. This formulation has been successfully applied to smooth-body separation and pressure-gradient flows (Whitmore *et al.* 2021, 2022, 2024). Although there are sensitivities in the solutions thus obtained with respect to the prescription of the slip lengths, it is possible to robustly obtain separated flow solutions at coarse grid resolutions in a variety of test cases.

Unlike the nonequilibrium models described above, slip wall models allow for a finite, nonzero wall-normal velocity (transpiration) at the wall, although its expression is typically prescribed rather than derived. In this study, we examine wall transpiration derived from Lighthill's (1958) analysis as a means to predict separated solutions at coarse resolutions. The advantage of this transpiration framework over existing methodologies is that it provides a conceptually simpler formulation, introducing a physically consistent wall-normal velocity that enables a Reynolds-number-independent mechanism for predicting separation.

The rest of this brief is organized as follows. Section 2 introduces an alternative derivation of the LES wall boundary condition as given by Lighthill (1958). Section 3 presents some preliminary solutions of the flow over the NASA/Boeing Gaussian bump. Concluding remarks are offered in Section 4.

2. Methodology

Most asymptotic analyses of boundary conditions used for WMLES consider the limit of infinite (or DNS) resolution; specifically, the boundary conditions reduce to no penetration ($v = 0$) and no-slip limits ($\tau_w = \mu(du/dn)$). However, we are also concerned with the behavior of the WMLES at coarse grid resolutions when the grid resolution is comparable to the thickness of the boundary layer ($\Delta \sim \delta$). The limit of this coarse grid LES is when the boundary layer thickness becomes subgrid to the interior LES ($\Delta > \delta$). In this limit, there is nothing that distinguishes the WMLES from an inviscid solution in the

vicinity of the wall, and the effects of the viscous boundary layer are encapsulated in the boundary condition of the wall. Lighthill (1958) derived the structure of the boundary condition necessary for the solution to capture the viscous effects on the outer, inviscid flow regimes. We repeat his derivation below and then extend it in the LES limit where the grid can resolve the boundary layer.

Consider a flow developing over a surface, where (u, v) denotes the viscous solution of the Navier–Stokes equations and (U_e, V_e) is the corresponding (inviscid) outer solution in the mean. For simplicity, we present the derivation in the context of flows that are two-dimensional in the mean, but the analysis can be extended to three-dimensional base flows as well. We impose the constraint that the two solutions are matched for all locations outside of the boundary layer,

$$U_e(x_i) = u(x_i), V_e(x_i) = v(x_i), \quad \forall x_i \notin X_\delta, \tag{2.1}$$

where X_δ is the region of space within the boundary layer. There is no requirement that the two solutions match within the boundary layer, $x \in X_\delta$. Both u, v and U_e, V_e satisfy the mean continuity equation

$$\frac{\partial U_e}{\partial x} + \frac{\partial V_e}{\partial y} = 0, \tag{2.2}$$

$$\frac{\partial u}{\partial x} + \frac{\partial v}{\partial y} = 0. \tag{2.3}$$

By subtracting Eq. (2.3) from Eq. (2.2) and integrating from the wall ($y = 0$) to the boundary layer edge ($y = \delta$), we obtain

$$\int_0^\delta \frac{\partial (U_e - u)}{\partial x}\, dy + [V_e - v]_{y=\delta} = V_e(x, y = 0) - v(x, y = 0). \tag{2.4}$$

Using the matching conditions at $y = \delta$ and the no-penetration condition for the viscous solution $v(x, 0) = 0$, we then obtain

$$\int_0^\delta \frac{\partial (U_e - u)}{\partial x}\, dy = V_e(x, y = 0). \tag{2.5}$$

Applying Leibniz's rule to the first term yields

$$\frac{d}{dx}\int_0^\delta (U_e - u)\, dy = \int_0^\delta \frac{\partial (U_e - u)}{\partial x}\, dy + (U_e - u)\Big|_{y=\delta} \frac{d\delta}{dx}. \tag{2.6}$$

Since $U_e = u$ at $y = \delta$, the second term on the right-hand side is identically zero, yielding

$$\frac{d}{dx}\int_0^\delta (U_e - u)\, dy = V_e(x, y = 0). \tag{2.7}$$

Defining the displacement thickness as

$$\delta^*(x) = \int_0^\delta \left(1 - \frac{u}{U_e}\right) dy, \tag{2.8}$$

we recover Lighthill's classic result:

$$\frac{d\,(U_e \delta^*)}{dx} = V_e(x, y = 0). \tag{2.9}$$

The result in Eq. (2.9) shows that in the limit when the boundary layer is subgrid, wall

transpiration is necessary for the outer flow to capture the impact of viscous effects. We now consider the case when the LES filter width (or grid resolution) can capture the boundary layer thickness ($\Delta < \delta$). We define the mean LES velocity components as U_Δ and V_Δ. We now apply a similar constraint to Eq. (2.1) to obtain

$$U_\Delta(x_i) = u(x_i), V_\Delta(x_i) = v(x_i), \quad \forall x_i \notin X_\Delta, \tag{2.10}$$

where X_Δ denotes the subgrid region adjacent to the wall, namely the portion of the flow below the LES filter width Δ that is not explicitly resolved. We can now map $\delta \mapsto \Delta$ in the Lighthill derivation above to yield

$$\frac{d}{dx}\int_0^\Delta (U_\Delta - u)\, dy = V_\Delta(x, y = 0). \tag{2.11}$$

We can see that the mean transpiration in Eq. (2.11) satisfies both asymptotic limits of infinite (DNS) and no (inviscid) resolution. If $\Delta \to 0$, then $V_\Delta = 0$ as the limit of the integral collapses. If $\Delta \geq \delta$, then $V_\Delta = V_e$, as defined in Eq. (2.9).

Equation (2.11) still does not comprise a closed model form: $u = u(x, y)$ (the DNS solution) is unknown, and the wall-normal integral of the LES solution, U_Δ, requires knowledge of the boundary condition on the tangential velocity field and its associated wall-normal profile. Nonetheless, it establishes that V_Δ may need to be finite. We can now show that Eq. (2.11) is equivalent to a slip wall model boundary condition if we admit the following approximations. Suppose that the LES filter width is constant along a particular surface. Then,

$$\begin{aligned} V_\Delta(x, y = 0) = \frac{d}{dx}\int_0^\Delta (U_\Delta - u)\, dy = \Delta \frac{d}{dx}\int_0^1 [U_\Delta - u]\, d\left(\frac{y}{\Delta}\right), \\ \approx -C\Delta\frac{dU_\Delta}{dx} = C\Delta\frac{dV_\Delta}{dy}, \end{aligned} \tag{2.12}$$

where C is a dimensionless prefactor that encapsulates the subgrid displacement thickness relative to the local grid scale Δ. In the implementation, the tangential velocity components (U_Δ and W_Δ) are set to zero at the wall, while the wall-normal component is prescribed according to Eq. (2.11). The resulting formulation is referred to as the transpiration model (TM).

2.1. *Flow solver*

All simulations are performed using charLES, an explicit unstructured finite-volume solver for the compressible Navier–Stokes equation (Brès *et al.* 2022). The solver employs Voronoi-based meshes and is formally second-order accurate in space and third-order accurate in time. Formally skew-symmetric spatial operators are used to ensure kinetic energy conservation, and the discrete formulation approximately preserves entropy in the inviscid, adiabatic limit. The unresolved turbulent scales are represented using the dynamic Smagorinsky model, where the model coefficient is locally averaged in time to ensure numerical stability (Germano *et al.* 1991; Lilly 1992).

This study employs an algebraic form of the EQWM to provide the tangential stress closure based on the Spalding (1961) law. We employ a first-point matching procedure, which has been shown to avoid log-layer mismatch in turbulent channel flows within the range $1000 \leq Re_\tau \leq 4200$ for standard LES grid resolutions.

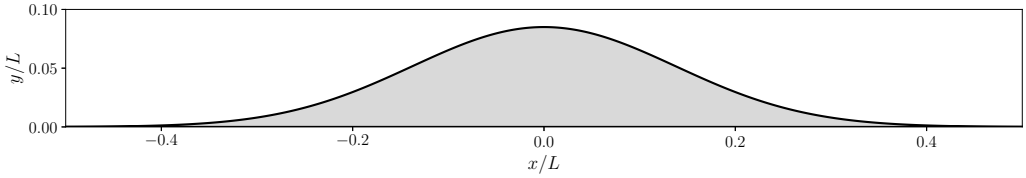

FIGURE 1. Two-dimensional Gaussian bump profile defined by Eq. (3.1), showing the streamwise (x) and wall-normal (y) coordinates and the normalized height h/L.

3. Simulations of the NASA/Boeing bump

3.1. *NASA/Boeing Gaussian bump*

Initial investigations into the validity of the assumptions underlying Lighthill's approximation are conducted on the two-dimensional Boeing Gaussian bump configuration, a canonical smooth-body separation problem introduced by Williams *et al.* (2020), further characterized experimentally by Gray *et al.* (2021, 2022), and subsequently used in several DNS (Uzun & Malik 2022) and WMLES studies (Whitmore *et al.* 2021, 2022, 2024; Agrawal *et al.* 2022, 2024a). The geometry represents a smooth surface that induces both favorable and adverse pressure gradients, resulting in separation and reattachment of the turbulent boundary layer.

The bump profile is defined analytically as

$$h(x) = h_0 \exp\left[-\left(\frac{x}{x_0}\right)^2\right], \tag{3.1}$$

where x is the streamwise coordinate, $h_0 = 0.085L$ is the maximum height, $x_0 = 0.195L$ controls the Gaussian decay, and L denotes the bump width. The geometry of the bump is illustrated in Figure 1. This configuration generates strong acceleration followed by an adverse pressure gradient downstream of the crest, leading to flow separation that becomes insensitive to Reynolds number at high Re_L (Williams *et al.* 2020).

The flow conditions follow Agrawal *et al.* (2024a) for the spanwise-periodic configuration at a reference Reynolds number,

$$Re_L \equiv \frac{U_\infty L}{\nu} = 2 \times 10^6, \tag{3.2}$$

based on the bump width L, the freestream velocity U_∞, and the kinematic viscosity ν. The quantities of interest are the skin-friction and pressure coefficients,

$$C_f = \frac{\tau_w}{\frac{1}{2}\rho_\infty U_\infty^2}, \qquad C_p = \frac{p - p_{\mathrm{ref}}}{\frac{1}{2}\rho_\infty U_\infty^2}, \tag{3.3}$$

where p_{ref} is taken in the upstream zero-pressure-gradient region.

Three simulations using the standard algebraic wall model (AWM) (Spalding 1961) were first performed to examine the grid-resolution requirements for accurately predicting smooth-body separation. The grid configurations follow Agrawal *et al.* (2024a, Table I) and include a coarse, a medium, and a fine mesh with approximately $N_{\mathrm{cv}} \approx 3 \times 10^6$, 1.2×10^7, and 5.2×10^7 control volumes, respectively. All grids have a maximum cell size of $\max(\Delta_{\mathrm{grid}}/L) = 0.01$, while the minimum wall-normal spacings are

$$\min(\Delta_{\mathrm{grid}}/L) = 1.3 \times 10^{-3} \text{ (coarse)},\ 6.3 \times 10^{-4} \text{ (medium)},\ \text{and } 3.1 \times 10^{-4} \text{ (fine)}.$$

Here, Δ_{grid} denotes the local grid resolution, which is distinct from the symbol Δ used

below to represent the distance from the wall to the first cell center in the transpiration formulation. At the inlet ($x/L = -1$), a uniform plug profile is prescribed. A nonreflecting freestream condition is applied at the top boundary, and a Navier–Stokes characteristic boundary condition is used at the outlet located at $x/L = 2.5$.

Various modeling approaches have been applied to this configuration, but reproducing the correct separation bubble size on the coarsest grid remains challenging (see Arranz *et al.* 2024 for a machine-learning-based wall-modeling paradigm that achieves reasonable predictions of flow separation on similarly coarse grids). In this study, simulations including wall transpiration are likewise restricted to this coarse grid to assess whether a transpiration velocity distribution can yield an accurate solution.The quasi-DNS data of Uzun & Malik (2022) were used to help evaluate the transpiration velocity in Eq. (2.11). The integral term in the equation was decomposed into two components: one computed *a priori* from the mean quasi-DNS data, denoted as g_{DNS}, and one evaluated during the LES, denoted as g_{LES}. These lead to the expression

$$\frac{d}{dx}\int_0^{\Delta}(U_{\Delta}-u)\,dy = \frac{d}{dx}\int_0^{\Delta}U_{\Delta}\,dy - \frac{d}{dx}\int_0^{\Delta}u\,dy = g_{\mathrm{LES}} - g_{\mathrm{DNS}}. \tag{3.4}$$

The g_{DNS} term was obtained prior to the LES using the quasi-DNS velocity fields and smoothed with a one-dimensional Gaussian filter to remove small-scale oscillations. As mentioned above, g_{LES} is itself unclosed, so for this investigation, we attempt a closure of the form

$$V_{\Delta} = \Delta\frac{dU_{\Delta}}{ds} - g_{\mathrm{DNS}}, \tag{3.5}$$

where Δ is the distance from the wall to the first cell center. To define the local wall-aligned (s, n) coordinate system, the wall-normal unit vector $\hat{\mathbf{n}}$ is obtained from the face normal. The streamwise reference direction $\mathbf{e}_x$ is projected onto the wall plane by removing its wall-normal component, yielding

$$\mathbf{t} = \mathbf{e}_x - (\mathbf{e}_x\cdot\hat{\mathbf{n}})\,\hat{\mathbf{n}}, \qquad \hat{\mathbf{t}} = \frac{\mathbf{t}}{\|\mathbf{t}\|}, \tag{3.6}$$

where $\hat{\mathbf{t}}$ defines the local tangential (streamwise) direction within the wall plane.

3.2. *Results*

Figure 2(a,b) shows the distributions of pressure and skin-friction coefficients, C_p and C_f, respectively, obtained using the AWM. The model does not predict the flattening of C_p, a symptom of flow separation, on either the coarse or the medium grid. Furthermore, the results exhibit nonmonotonic grid convergence, as the coarse grid performs slightly better than the medium one—particularly in C_f, where a small region of negative skin friction appears downstream of the bump crest. Separation is captured only on the finest grid, where the viscous pressure-gradient-induced sublayer is marginally resolved (see Agrawal *et al.* 2024a for details).

The results obtained with wall transpiration are compared with those from the AWM at the coarsest resolution in Figure 3(a,b) for C_p and C_f, respectively. The inclusion of wall transpiration yields a clear improvement over the AWM in both pressure and skin-friction distributions, enabling the recovery of a separated flow and a more realistic overall behavior. However, the detailed shape of the separation region is not captured exactly—the C_p distribution exhibits a reduced plateau, and the C_f shows a milder dip compared with the DNS. In addition, the reattachment point occurs somewhat earlier

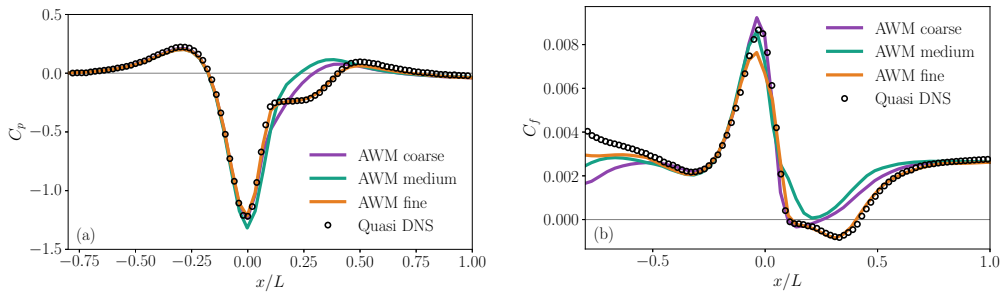

FIGURE 2. Time-averaged (a) pressure coefficient and (b) skin-friction coefficient obtained using the AWM for grid-convergence assessment versus quasi-DNS for coarse, medium, and fine grids.

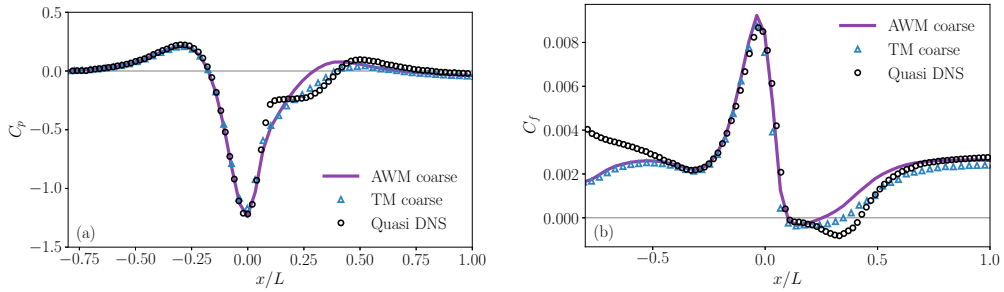

FIGURE 3. Time-averaged (a) pressure coefficient and (b) skin-friction coefficient comparing the AWM (coarse grid) with the TM (coarse grid) against quasi-DNS.

than in the reference data, although the overall agreement remains better than that obtained with the AWM.

Figure 4 shows the streamwise distribution of the transpiration velocity. The velocity is negative (suction) in the region of favorable pressure gradient and positive (blowing) in the region of adverse pressure gradient. Results at this juncture are not yet predictive, but they demonstrate that a reasonable solution can be obtained from the introduction of wall transpiration.

4. Conclusions

The prediction of separation and reattachment in turbulent boundary layers due to mild pressure gradients has been a continued challenge for WMLES. The required resolutions used to capture these phenomena are often prohibitive in the context of practical engineering flows. To address these concerns, we derive a form of LES boundary conditions that rely on two constraints: the continuity equation and the fact that the LES solution matches the Navier–Stokes (DNS) solution in the region beyond the filter width. We show that satisfying these two constraints necessitates a finite wall transpiration velocity in the mean. Moreover, the derived form of the transpiration velocity is asymptotically consistent with the solution for the outer flow when the boundary layer is unresolved and recovers Lighthill's result in this limit. Finally, we show that, under certain assumptions, this boundary condition is equivalent to the application of a slip wall model (for the wall-normal velocity) in the mean.

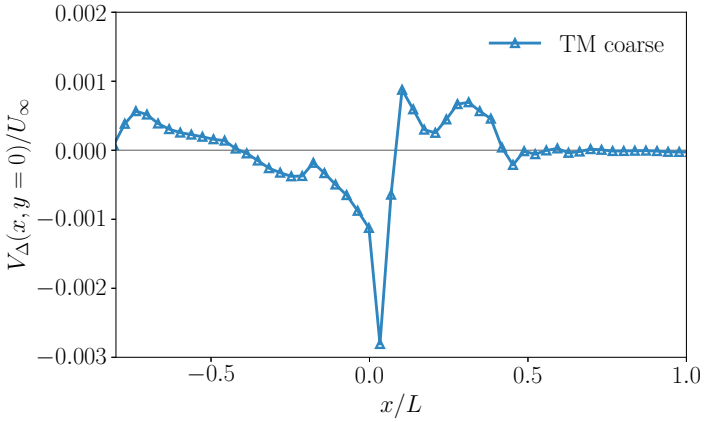

FIGURE 4. Streamwise distribution of the normalized transpiration velocity, V_Δ/U_∞, where U_∞ is the freestream velocity.

To demonstrate the potential for a boundary condition of this form, WMLES of the NASA/Boeing Guassian bump were performed. The inclusion of wall transpiration yields an improvement in both pressure and skin-friction distributions, exhibiting separated flow behavior. Although the separation region is not captured exactly—with a reduced C_p plateau, milder C_f dip, and slightly earlier reattachment—the overall agreement represents an improvement over the AWM. The model as presented is not yet fully predictive, as the computation of the particular wall transpiration velocity distribution is aided by the availability of quasi-DNS data. The construction of the predictive model form will be the subject of future work.

Acknowledgments

Support from the Office of Naval Research to the Center for Turbulence Research (grant N000142312833) is gratefully acknowledged. This research used resources of the Oak Ridge Leadership Computing Facility at the Oak Ridge National Laboratory, which is supported by the Office of Science of the US Department of Energy under contract DE-AC05-00OR22725.

REFERENCES

AGRAWAL, R., BOSE, S. T. & MOIN, P. 2024a Reynolds-number-dependence of length scales governing turbulent-flow separation in wall-modeled large eddy simulation. *AIAA J.* **62**, 3686–3699.

AGRAWAL, R., BOSE, S. T. & MOIN, P. 2024b Nonequilibrium wall model for large-eddy simulations of complex flows exhibiting turbulent smooth-body separation. *Phys. Rev. Fluids* **9**, 124603.

AGRAWAL, R., WHITMORE, M. P., GRIFFIN, K. P., BOSE, S. T. & MOIN, P. 2022 Non-Boussinesq subgrid-scale model with dynamic tensorial coefficients. *Phys. Rev. Fluids* **7**, 074602.

ARRANZ, G., LING, Y., COSTA, S., GOC, K. & LOZANO-DURÁN, A. 2024 Building-block-flow computational model for large-eddy simulation of external aerodynamic applications. *Commun. Eng.* **3**, 127.

Bae, H. J., Lozano-Durán, A., Bose, S. T. & Moin, P. 2019 Dynamic slip wall model for large-eddy simulation. *J. Fluid Mech.* **859**, 400–432.

Balaras, E., Benocci, C. & Piomelli, U. 1996 Two-layer approximate boundary conditions for large-eddy simulations. *AIAA J.* **34**, 1111–1119.

Bose, S. T. & Moin, P. 2014 A dynamic slip boundary condition for wall-modeled large-eddy simulation. *Phys. Fluids* **26**, 015104.

Brès, G. A., Bose, S. T., Ivey, C. B., Emory, M. & Ham, F. 2022 GPU-accelerated large-eddy simulations of supersonic jets from twin rectangular nozzles. *AIAA Paper 2022-3001*.

Cabot, W. & Moin, P. 1999 Approximate wall boundary conditions in the large-eddy simulation of high Reynolds number flow. *Flow, Turbul. Combust.* **63**, 269–291.

Choi, H. & Moin, P. 2012 Grid-point requirements for large-eddy simulation: Chapman's estimates revisited. *Phys. Fluids* **24**, 011702.

Fowler, M., Zaki, T. A. & Meneveau, C. 2022 A Lagrangian relaxation towards equilibrium wall model for large-eddy simulation. *J. Fluid Mech.* **934**, A44.

Fowler, M., Zaki, T. A. & Meneveau, C. 2023 A multi-time-scale wall model for large-eddy simulations and applications to non-equilibrium channel flows. *J. Fluid Mech.* **974**, A51.

Germano, M., Piomelli, U., Moin, P. & Cabot, W. H. 1991 A dynamic subgrid-scale eddy viscosity model. *Phys. Fluids A* **3**, 1760–1765.

Gray, P. D., Gluzman, I., Thomas, F., Corke, T., Lakebrink, M. & Mejia, K. 2021 A new validation experiment for smooth-body separation. *AIAA Paper 2021-2810*.

Gray, P. D., Gluzman, I., Thomas, F. O., Corke, T. C., Lakebrink, M. T. & Mejia, K. 2022 Benchmark characterization of separated flow over a smooth Gaussian bump. *AIAA Paper 2022-3342*.

Lighthill, M. J. 1958 On displacement thickness. *J. Fluid Mech.* **4**, 383–392.

Lilly, D. K. 1992 A proposed modification of the Germano subgrid-scale closure method. *Phys. Fluids A* **4**, 633–635.

Park, G. I. & Moin, P. 2014 An improved dynamic non-equilibrium wall model for large-eddy simulation. *Phys. Fluids* **26**, 015108.

Spalding, D. B. 1961 A single formula for the "law of the wall." *J. Appl. Mech.* **28**, 455–458.

Uzun, A. & Malik, M. R. 2022 A dynamic nonlinear subgrid-scale model for large-eddy simulation of complex turbulent flows. Tech. Memo. 20220013891, NASA Langley Research Center.

Whitmore, M. P., Bose, S. T. & Moin, P. 2022 Progress on slip wall-modeled LES for predicting smooth-body separation. *Annual Research Briefs*, Center for Turbulence Research, Stanford University, pp. 59–70.

Whitmore, M. P., Bose, S. T. & Moin, P. 2023 Evaluation of an optimal slip wall model for large-eddy simulation. *Annual Research Briefs*, Center for Turbulence Research, Stanford University, pp. 283–294.

Whitmore, M. P., Bose, S. T. & Moin, P. 2024 Application of a sensor-based slip wall model in the presence of pressure-gradient effects. *Annual Research Briefs*, Center for Turbulence Research, Stanford University, pp. 219–229.

Whitmore, M. P., Griffin, K. P., Bose, S. T. & Moin, P. 2021 Large-eddy sim-

ulation of a Gaussian bump with slip-wall boundary conditions. *Annual Research Briefs*, Center for Turbulence Research, Stanford University, pp. 45–58.

Williams, O., Samuell, M., Sarwas, E. S., Robbins, M. & Ferrante, A. 2020 Experimental study of a CFD validation test case for turbulent separated flows. *AIAA Paper 2020-0092*.

Yang, X. I. A. & Griffin, K. P. 2021 Grid-point and time-step requirements for direct numerical simulation and large-eddy simulation. *Phys. Fluids* **33**, 015108.